Electromagnetic generation of gigahertz sound in ferromagnetic metals

G. Dewar
Department of Physics, University of Miami, P.O. Box 248046 Coral Gables, Florida 33124
(Received 25 June 1987)

Calculations of the transmission of ultrasonic energy through ferromagnetic metallic slabs in the normal conductivity regime have been compared with experimental results. The longitudinal sound was generated by incident microwaves at the slab's front surface and subsequently detected by the reemission of microwaves at the back surface. The configuration studied was the one in which the applied magnetic field and microwave magnetic field were parallel and both were in the slab's plane. The sound was generated through the stress arising from the inhomogeneous Zeeman energy at the slab's surface. The reemission at the back surface was proportional to the volume magnetostriction and bulk modulus. Neither the magnetoelastic constants B_1 and B_2, the imbalance between the Lorentz force and the electronic collision force on the lattice, nor the antisymmetric stress tensor terms played a significant role in the transmission. Comparison of the calculation to experimental data on iron indicate that the electronic attenuation of 9.4-GHz longitudinal sound is ≈ 0.05 dB/μm at room temperature. The experimental data also suggest that work hardening iron tends to increase the volume magnetostriction appreciably.

I. INTRODUCTION

This paper deals with the interconversion of microwaves and sound waves in ferromagnetic metals. The emphasis is on the configuration in which the microwave magnetic field is parallel to the static magnetic field and both fields lie in the plane of the sample surface. This is known as the parallel-parallel configuration. The case where these fields are perpendicular is well understood.[1-3]

The coupling between microwaves and sound waves arises from four sources: (1) the spatially inhomogeneous Zeeman energy which gives rise to a force on the lattice, (2) the magnetoelastic coupling, (3) the imbalance between the Lorentz force and the electronic collision force on the lattice, and (4) the interchange of angular momentum between the magnetization and the lattice. The results of the calculations and comparison to experiment which follow show that the dominant source of coupling for the parallel-parallel configuration is the inhomogeneous Zeeman energy. The magnetoelastic coupling constants B_1 and B_2 relating magnetization direction to strain are relatively inconsequential in the parallel-parallel configuration. This follows from the fact that the radio-frequency magnetic field is parallel to the magnetization and cannot exert a torque which would change the magnetization direction. The volume magnetostriction, however, plays an important role in the conversion of sound to microwaves. The other two types of coupling are relatively ineffective for the materials and frequencies considered.

The aim of this paper is to formulate a description of the experiments of Alexandrakis and co-workers[4-6] and to understand some of the experimental results obtained by Blackstead and co-workers.[7,8] The background for this description has been developed by Tiersten,[9] by Vittoria, Bailey, Barker, and Yelon,[10] by Kobayashi, Barker, Bleustein, and Yelon,[11] and by Vittoria, Craig, and Bailey.[12] In the experiment[4,5] a slab of ferromagnetic material forms the common wall between two microwave cavities. Microwaves are incident on one cavity. Any energy which passes through the slab and is radiated into the second cavity is sampled by a detector. The magnetic field dependence, temperature dependence, and the amplitude of the transmission signal can be calculated and compared to experiment.

The outline of this paper is as follows. Immediately following is a description of the model used in the calculation. Next, the equations of motion appropriate to the model are developed and then the boundary conditions arising from these equations are derived. After an outline of how the transmission calculation is carried out, the simple case of transmission through a thick slab is considered. Finally, detailed comparisons of the calculation are made to experiments on iron.

II. MODEL

The subsequent sections develop the equations which describe a three-constituent model for the ferromagnetic metal. These constituents are the elastic medium, the magnetic continuum, and the conduction-electron system. Previous developments of magnetoelastic descriptions of magnetic media at microwave frequencies applied to nonconductors and have ignored the conduction electrons[9,11] except for the use of a scalar conductivity in Ohm's law.[1,2,4,5,10,12] The development here follows from the application of Maxwell's equations and the laws of conservation of mass, linear momentum, and angular momentum to an arbitrary volume element of the coupled elastic, magnetic, and conduction-electron systems under the assumption that the medium is responding to a small dynamic field.

The elastic medium is assumed to obey Hooke's law and to be adequately described by the macroscopic strain field $\mathbf{u}=\mathbf{u}_0\exp(ikx-i\omega t)$. This represents a wave

moving in the x direction with propagation constant k and angular frequency ω. The magnetic continuum has a magnetization $\mathbf{M}$ which cannot move relative to the elastic medium. This is essentially a localized model for the magnetization. The magnetic moment per ion is not assumed fixed but is dictated by the equation of state for the magnetization. The conduction electrons are described by the free-electron theory. The mean free path for electrons is taken to be much shorter than the length associated with waves in the material, and the mean free time between collisions is much less than $1/\omega$.

The sample geometry for the calculation is presented in Fig. 1. The sample slab is infinite in the y and z directions and of thickness d. The normal to the slab is along the [110] crystal direction and the applied static and radio-frequency magnetic fields are applied along the z direction, which coincides with the $[1\bar{1}1]$ direction in the crystal.

III. EQUATIONS OF MOTION

The description of the response of a slab of ferromagnetic metal to electromagnetic radiation is formulated below. The electromagnetic fields inside the material must, of course, obey Maxwell's equations. The form of Maxwell's equations used here is

$$\nabla\times\mathbf{H}=\frac{4\pi\mathbf{J}}{c}+\frac{1}{c}\frac{\partial(\epsilon\mathbf{E})}{\partial t} \tag{1}$$

and

$$\nabla\times\mathbf{E}=-\frac{1}{c}\frac{\partial\mathbf{B}}{\partial t} \quad \text{where } \mathbf{B}=\mathbf{H}+4\pi\mathbf{M} \ . \tag{2}$$

The notation used for fields is, for example, $\mathbf{H}=\mathbf{H}_0+\mathbf{h}\exp(ikx-i\omega t)$ where $\mathbf{H}$ is the total magnetic field, $\mathbf{H}_0$ is the static magnetic field, and $\mathbf{h}$ is the amplitude of the (assumed small) oscillating magnetic field. A similar notation applies to the total current $\mathbf{J}$, the electric field $\mathbf{E}$, the magnetization $\mathbf{M}$, and the magnetic induction $\mathbf{B}$.

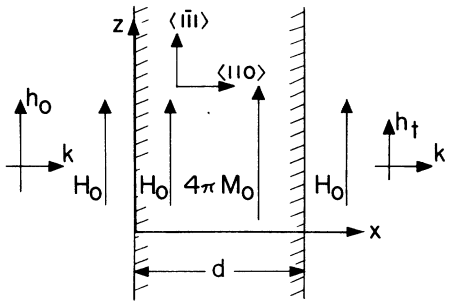

FIG. 1. Sketch of coordinate axes and crystal orientation used in the calculation. The x axis is normal to the semi-infinite slab of thickness d. The applied, static magnetic field $\mathbf{H}_0$, the static magnetization $4\pi\mathbf{M}_0$, and the incident and transmitted microwave fields $\mathbf{h}_0$ and $\mathbf{h}_t$ are parallel to the z axis. $\mathbf{k}$ is the waves' propagation constant and is parallel to the x axis. The crystal is oriented so that the [110] direction is parallel to the x axis and the $[1\bar{1}1]$ direction is parallel to the z axis.

The magnitude of the magnetization has a small oscillating component which is driven by the strain field and the magnetic field. Previous authors[9,12] have assumed that the magnetic moment per ion is fixed and, since there is a volume change associated with a longitudinal sound wave, the oscillating magnetization is

$$m_z=-M_0\frac{\partial u_x}{\partial x} \ ,$$

where M_0 is the static saturation magnetization. This is not a good assumption. The volume magnetostriction in bulk iron gives rise to a term of comparable size and in invar a term an order of magnitude larger.

The equation of state for the magnetic moment can be considered a function of magnetic field, volume, and entropy. Small changes in the magnetic moment can be expressed as

$$d\mu=\left[\frac{\partial\mu}{\partial H}\right]_{V,S}dH+\left[\frac{\partial\mu}{\partial V}\right]_{H,S}dV+\left[\frac{\partial\mu}{\partial S}\right]_{V,H}dS \ , \tag{3}$$

where μ, V, and S are the magnetic moment, volume, and entropy, respectively. The magnetic moment attains its equilibrium value in a time[13] $\approx 1/\omega_{ex}$ where ω_{ex} is the exchange frequency and is much higher than the wave frequency ω. Thus the magnetic moment is determined by the instantaneous values of H, V, and S. The frequency is also low enough that the waves propagate under adiabatic conditions so that $dS=0$. After some standard manipulation of thermodynamic quantities, and noting that

$$m_z=d\left[\frac{\mu}{V}\right]=\frac{d\mu}{V}-\frac{\mu}{V}\frac{\partial u_x}{\partial x} \ ,$$

then

$$m_z=\left\{\chi+\left[\frac{1}{V}\left[\frac{\partial V}{\partial H}\right]_{P,S}\right]^2 V\left[\frac{\partial P}{\partial V}\right]_{H,S}\right\}h_z + [(\beta-1)M_0]\frac{\partial u_x}{\partial x} \ . \tag{4}$$

The susceptibility used in Eq. (4) is

$$\chi=\frac{1}{V}\left[\frac{\partial\mu}{\partial H}\right]_{P,S} \tag{5}$$

and the volume magnetostriction, usually measured under conditions of constant pressure and temperature, is

$$\frac{1}{V}\left[\frac{\partial V}{\partial H}\right]_{P,S}=\frac{1}{V}\left[\frac{\partial V}{\partial H}\right]_{P,T}+\frac{T\alpha}{C_P}\left[\frac{\partial\mu}{\partial T}\right]_{H,P} \ . \tag{6}$$

In Eq. (6) T is the temperature, C_P is the specific heat at constant pressure and field, and α is the coefficient of volume expansion. The appropriate bulk modulus in Eq. (4) is calculated under the assumption that the crystal is free to move in the [110] direction only. Then

$$V\left[\frac{\partial P}{\partial V}\right]_{H,S}=-(C_{11}+C_{12}+2C_{44})/2\ , \tag{7}$$

where the C_{ij}'s are the elastic constants. β is a convenient parametrization of the volume magnetostriction, namely

$$\beta=-\frac{1}{M_0}\frac{1}{V}\left[\frac{\partial V}{\partial H}\right]_{P,S}V\left[\frac{\partial P}{\partial V}\right]_{H,S}\ . \tag{8}$$

The transverse response of the magnetization can be conveniently described by the Landau-Lifshitz equation of motion for the magnetization as modified by Gilbert:

$$\frac{\partial \mathbf{M}}{\partial t}=-\gamma(\mathbf{M}\times\mathbf{H}_{\text{eff}})+\frac{\lambda}{\gamma M_0^2}\left[\mathbf{M}\times\frac{\partial \mathbf{M}}{\partial t}\right]\ . \tag{9}$$

Here $\gamma=|ge/2mc|$ and g is the spectroscopic splitting factor, λ is the phenomenological damping parameter, and $\mathbf{H}_{\text{eff}}$ is the effective field which gives rise to the torque on the magnetization. $\mathbf{H}_{\text{eff}}$ includes contributions from the applied magnetic field, the demagnetizing field, the exchange energy, the magnetic anisotropy, and the magnetoelastic energy.[12] (Although the demagnetizing energy in this configuration is zero, the calculation is easily modified to describe an ellipsoidal sample mounted in a cavity wall for which this energy is nonzero.[14,15]) After Eq. (9) is linearized and the terms proportional to $\exp(ikx-i\omega t)$ extracted,

$$-\frac{1}{\gamma}\frac{\partial m_x}{\partial t}\left[H_0-4\pi D_{zz}M_0-\frac{2A}{M_0}\frac{\partial^2}{\partial x^2}-\left[\frac{4K_1}{3M_0}+\frac{4K_2}{9M_0}\right]+\left[\frac{\lambda}{\gamma^2M_0}\right]\frac{\partial}{\partial t}\right]m_y+\frac{\sqrt{2}}{3}(B_1-B_2)\frac{\partial u_x}{\partial x}+M_0h_y=0 \tag{10}$$

and

$$\left[H_0+4\pi(1-D_{zz})M_0-\frac{2A}{M_0}\frac{\partial^2}{\partial x^2}-\left[\frac{4K_1}{3M_0}+\frac{4K_2}{9M_0}\right]+\left[\frac{\lambda}{\gamma^2M_0}\right]\frac{\partial}{\partial t}\right]m_x-\frac{1}{\gamma}\frac{\partial m_y}{\partial t}-\frac{\sqrt{2}}{3}(B_1-B_2)\frac{\partial u_y}{\partial x}$$
$$+\tfrac{1}{3}(2B_1+B_2)\frac{\partial u_z}{\partial x}-M_0h_x=0\ . \tag{11}$$

In Eqs. (10) and (11) D_{zz} is the demagnetization factor, A is the exchange stiffness constant, the K_i's are the anisotropy constants, and the B_i's are the magnetoelastic coupling constants.

The equation of motion for the elastic continuum is essentially the expression of conservation of momentum and of angular momentum for the medium.[9,12] The equations developed here are similar to those of Vittoria *et al.*[12] but augmented by four types of terms. First, a body force which arises from the spatially inhomogeneous Zeeman energy, $\nabla(\mathbf{M}\cdot\mathbf{B})$, is incorporated into the equation. This force is present for both metallic and nonconducting ferromagnets and can be thought of as the Lorentz force acting on the magnetic moment of the medium. To avoid confusion with the usual Lorentz force this will be referred to as the Zeeman force. Inclusion of this type of term in the equation of motion for the elastic continuum is a major contribution of Privorotskii,[16] although his stress tensor also included a force which was nonzero for the empty magnetic lattice and should not be included here. Second, the lattice is charged and, hence, subject to the Lorentz force in its usual form:

$$\mathbf{F}_{Lz}=-ne\left[\mathbf{E}+\frac{1}{c}\frac{\partial \mathbf{u}}{\partial t}\times(\mathbf{H}+4\pi\mathbf{M})\right]\ . \tag{12}$$

Here, n is the number of conduction electrons per unit volume, e is the charge carried by each electron, and $\mathbf{F}_{Lz}$ is the Lorentz force per unit volume. Third, the conduction electrons dump momentum into the background elastic continuum during collisions. This collision force tends to cancel the effect of the Lorentz force but this combination of forces gives rise to the direct electromagnetic generation of sound in the presence of a magnetic field at megahertz frequencies.[17] Fourth, conservation of angular momentum requires that antisymmetrical stress tensor terms exist whenever the magnitude of the magnetic moment per ion changes with time.

The x-coordinate equation of motion for the elastic medium is

$$\left[\frac{(C_{11}+C_{12}+2C_{44})}{2}\frac{\partial^2}{\partial x^2}-\rho\frac{\partial^2}{\partial t^2}\right]u_x-\frac{\sqrt{2}}{3}\left[\frac{B_1-B_2}{M_0}\right]\frac{\partial m_y}{\partial x}+M_0\frac{\partial h_z}{\partial x}+H_0\frac{\partial m_z}{\partial x}$$
$$-ne\left[e_x+\left[\frac{1}{c}\frac{\partial \mathbf{u}}{\partial t}\times(\mathbf{H}_0+4\pi\mathbf{M}_0)\right]_x\right]+(F_x)_{\text{coll}}=0\ . \tag{13}$$

The first term in Eq. (13) is simply an expression of Newton's second law for the unadorned elastic medium[18] where ρ is the mass density. The C_{ij}'s can have a small imaginary part incorporated into them to phenomenologically account for elastic damping.[9] The remaining terms correspond to additional forces on the lattice. The second term represents the magnetoelastic coupling. The third and fourth terms represent the Lorentz force arising from the inhomogeneous Zeeman energy. The fifth term is the Lorentz force acting on the conduction electrons and the lattice. The last term is the force on the lattice due to collisions with conduction electrons and equals the average rate momentum is lost by these electrons. Only terms linear in small quantities have been retained.

The equations of motion for the y and z directions are

$$\left[\frac{(C_{11}-C_{12}+4C_{44})}{6}\frac{\partial^2}{\partial x^2}-\rho\frac{\partial^2}{\partial t^2}\right]u_y-\frac{\sqrt{2}(C_{11}-C_{12}-2C_{44})}{6}\frac{\partial^2 u_z}{\partial x^2}-\frac{\sqrt{2}}{3}\left[\frac{B_1-B_2}{M_0}\right]\frac{\partial m_x}{\partial x}$$
$$-\frac{1}{2\gamma' V}\frac{\partial^2\mu_z}{\partial x\,\partial t}-ne\left[e_y+\left[\frac{1}{c}\frac{\partial \mathbf{u}}{\partial t}\times(\mathbf{H}_0+4\pi\mathbf{M}_0)\right]_y\right]+(F_y)_{\rm coll}=0 \quad (14)$$

and

$$\left[\frac{(C_{11}-C_{12}+C_{44})}{3}\frac{\partial^2}{\partial x^2}-\rho\frac{\partial^2}{\partial t^2}\right]u_z-\frac{\sqrt{2}(C_{11}-C_{12}-2C_{44})}{6}\frac{\partial^2 u_y}{\partial x^2}+\frac{1}{3}\left[\frac{2B_1+B_2}{M_0}\right]\frac{\partial m_x}{\partial x}-ne(e_z)+(F_z)_{\rm coll}=0\ . \quad (15)$$

In the fourth term of Eq. (14) $\gamma'=|g'e/2mc|$ where g' is the magnetomechanical factor one would measure in a Barnett experiment or an Einstein–de Haas experiment. This term is essentially the antisymmetrical component of the stress tensor which balances the angular momentum dumped into the lattice when the magnitude of the magnetic moment per ion changes.

The conduction-electron force on the lattice and the conductivity are calculated in the regime in which the electronic mean free path l and the mean free time between collisions, τ, are such that $(kl)^2<\omega\tau<1$. This allows the collision force to be calculated simply from the Boltzmann equation in the relaxation-time approximation by weighting the electronic distribution of states with the momentum carried by each state. In the coordinate frame attached to the lattice the collision force density is

$$\mathbf{F}'_{\rm coll}=\frac{nm}{\tau}\langle\mathbf{v}'\rangle=\frac{m}{e\tau}\mathbf{J}'_{\rm RM}\ . \quad (16)$$

The primes denote the fact that the fields must be evaluated in the accelerated coordinate system attached to the lattice. Here m is the mass of the electron and $\langle\mathbf{v}'\rangle$ is the average drift velocity of electrons relative to the lattice. This collision-force density can be rewritten by noting that $ne\langle\mathbf{v}'\rangle$ is the current due to relative motion of the conduction electrons and the lattice between the collisions, $\mathbf{J}'_{\rm RM}$. The collision force is trivially transformed to the laboratory frame in which Eqs. (13)–(15) are written, since $\mathbf{F}_{\rm coll}=\mathbf{F}'_{\rm coll}$. The transformation for $\mathbf{J}'_{\rm RM}$ is given implicitly below.

Similarly, the resistivity can be extracted from a Boltzmann equation describing the time evolution of the conduction-electron distribution under the influence of external fields. There is a complication due to the ferromagnetic Hall effect. Ferromagnetic metals are observed to have a contribution to the Hall constant which is much larger than that of ordinary metals and which scales in temperature with the resistivity squared. Berger[19] has pointed out that this effect can be described as a side step of the electron's wave packet of $\sim 10^{-8}$ cm during each collision. The origin of this side-step current, $\mathbf{J}_{\rm SS}$, is in the spin-orbit coupling. The total current, as viewed in the frame attached to the lattice, is

$$\mathbf{J}'=\mathbf{J}'_{\rm RM}+\mathbf{J}'_{\rm SS}\ \text{ with }\ \mathbf{J}'_{\rm RM}\perp\mathbf{J}'_{\rm SS}\ . \quad (17)$$

The linearized Boltzmann equation, in the relaxation-time approximation, for the electronic current is

$$\frac{\partial}{\partial t}\left[\frac{m}{e}\mathbf{J}'\right]=ne\mathbf{E}'+\frac{1}{c}[\mathbf{J}'\times(\mathbf{H}'+4\pi\mathbf{M}')]$$
$$-\frac{m}{e\tau}\mathbf{J}'_{\rm RM}-nm\frac{\partial^2\mathbf{u}}{\partial t^2}\ . \quad (18)$$

The third term on the right of Eq. (18) is the relaxation term and is essentially $-\mathbf{F}'_{\rm coll}$. The last term is the frame pseudoforce.

The side-step current is conveniently parametrized in terms of Λ, the ratio of the amplitude of the side step to the electronic mean free path:[19]

$$\mathbf{J}'_{\rm SS}=\Lambda\mathbf{J}'_{\rm RM}\times\left[\frac{\mathbf{B}'}{|\mathbf{B}'|}\right]\ . \quad (19)$$

Equation (19) can be transformed to laboratory frame variables by noting that, since the material has no net charge and there is no static electric field, $\mathbf{J}'=\mathbf{J}$ and $\mathbf{H}'+4\pi\mathbf{M}'=\mathbf{H}+4\pi\mathbf{M}$ to first order in small quantities. However, the electric field transforms according to

$$\mathbf{E}'=\mathbf{E}+\frac{1}{c}\frac{\partial\mathbf{u}}{\partial t}\times(\mathbf{H}_0+4\pi\mathbf{M}_0)\ . \quad (20)$$

After some manipulation, the relation between the

amplitudes of the oscillating electric field and the current can be expressed in the laboratory frame as

$$\mathbf{e}=\begin{bmatrix}(1-i\omega\tau)/\sigma & -\Lambda/\sigma-B/nec & 0\\ \Lambda/\sigma+B/nec & (1-i\omega\tau)/\sigma & 0\\ 0 & 0 & (1-i\omega\tau)/\sigma\end{bmatrix}\mathbf{j}+\begin{bmatrix}-i\omega m/e & -B/nec & 0\\ B/nec & -i\omega m/e & 0\\ 0 & 0 & -i\omega m/e\end{bmatrix}ne\frac{\partial\mathbf{u}}{\partial t}\ . \quad (21)$$

Here terms $\sim(\omega\tau)^2,\Lambda^2$ have been omitted. Also $\sigma=ne^2\tau/m$, and $\partial/\partial t$ has been selectively replaced by $-i\omega$.

Equation (21) is inconsistent with Eqs. (13)–(15) in that terms proportional to k^2 have been omitted from Eq. (21) whereas $\partial^2/\partial x^2=-k^2$ has been retained in Eqs. (13)–(15). The motivation for this omission is that this greatly simplifies the calculations which follow. Comparison to more general derivations of the conductivity by Kjeldaas and Holstein[20] and by Cohen, Harrison, and Harrison[21] show that the primary implication of this omission is that the diffusion current is not present in Eq. (21). If the conductivity were correct to order k^2 then terms which derive from the Fermi pressure would augment the C_{ij}'s in Eqs. (13)–(15). Further, some of the terms in the matrices of Eq. (21) would be modified by factors of $[1+s(kl)^2]$ where s is a numerical factor which ranges between $-\frac{2}{5}$ and $\frac{3}{5}$. Since the numerical calculations ultimately use experimentally measured values of the C_{ij}'s and the model chosen applies only if $(kl)^2\ll 1$ there are no difficulties in principle with this inconsistency.

The parameter Λ which characterizes the ferromagnetic Hall effect does not enter into the expression for the stress on the lattice. Substitution of Eqs. (16) and (21) into Eqs. (13)–(15) shows that the Lorentz and collision forces are

$$\mathbf{F}_{Lz}+\mathbf{F}_{coll}=-\begin{bmatrix}-i\omega m/e & -B/c & 0\\ B/c & -i\omega m/e & 0\\ 0 & 0 & -i\omega m/e\end{bmatrix}\mathbf{j}\ . \quad (22)$$

The reason for this absence is simply that no net momentum is acquired by electrons due to each side step and, hence, there is no force on the lattice.

This model does not require that the charge conservation condition be explicitly imposed. If charge conservation is required of the electrons and lattice separately, then one is led to equations which describe a longitudinal plasma wave with a propagation constant $|k|\approx 10^8$ cm^{-1}. This is too short a wavelength to be adequately described in this semiclassical model. In any event, inclusion of this wave in the calculations which follow would lead to insignificant quantitative changes.

Equations (1) and (2), (4), (10) and (11), (13)–(15), and (21) constitute a system of linear, homogeneous equations for **h**, **m**, **e**, **j**, and **u**. Setting the determinant of the coefficients equal to zero yields a seventh degree polynomial in k^2. The propagation constants correspond to seven pairs of forward and backward propagating waves. These waves can be regarded as two electromagnetic waves, two spin waves, and three sound waves. Several authors have analytically examined these propagation constants as functions of frequency or applied magnetic field.[11,12] The ordinary electromagnetic wave and the longitudinal sound wave are of primary interest in this paper. The relative changes in the magnitudes of these waves' propagation constants introduced by the coupling terms due to the Zeeman force, the Lorentz force, the volume magnetostriction, and the Hall conductivity are $\lesssim 10^{-3}$. This implies that, unlike the sound generation in the parallel-perpendicular configuration, the sound generation is not a resonance phenomenon associated with a dispersion relation crossing.

IV. BOUNDARY CONDITIONS AND TRANSMISSION CALCULATION

The boundary value problem we ultimately wish to solve is one in which an incident electromagnetic wave on one side of a semi-infinite slab gives rise to reflected and transmitted waves, of two possible polarizations each, and seven pairs of backward and forward propagating waves within the slab. These 18 wave amplitudes are determined relative to the incident wave from nine independent boundary conditions at the front and back surfaces of the slab. The boundary conditions simply assert that Maxwell's equations and the equations of motion hold at material discontinuities.

The boundary conditions for the tangential components of **e** and **h** are obtained in the usual manner by integrating the fields along a closed path traversing the boundary and then using Stokes' theorem. This results in the conditions that h_y, h_z, and e_z are continuous across the slab boundary. The boundary condition for e_y is complicated by the fact that the moving ferromagnet introduces an oscillating magnetic dipole moment at the surface. The time derivative of the surface dipole moment is $-M_0(\partial u_x/\partial t)$ and the boundary condition on e_y is

$$e_y^{out}=e_y^{in}-\left[\frac{4\pi M_0}{c}\right]\frac{\partial u_x}{\partial t}\ . \quad (23)$$

The superscripts in and out refer to fields inside or outside the material. Equation (23) can also be derived from Eq. (20) by noting that e_y' is continuous in the frame instantaneously at rest with the boundary and then transforming back to the laboratory frame.

The boundary conditions resulting from the equations of motion are determined by integrating Eqs. (10) and (11) and (13)–(15) along an interval which crosses the boundary, and then taking the limit as the interval's length shrinks to 0. This corresponds to conserving angular and linear momentum at the boundary and is commonly known as the spin unpinned, traction-free set of boundary conditions. These boundary conditions are

$$\frac{2A}{M_0^2}\frac{\partial m_y}{\partial x}+\frac{\sqrt{2}}{3}\left[\frac{B_1-B_2}{M_0}\right]u_x=0\ , \tag{24}$$

$$\frac{2A}{M_0}\frac{\partial m_x}{\partial x}+\frac{\sqrt{2}}{3}\left[\frac{B_1-B_2}{M_0}\right]u_y-\frac{1}{3}\left[\frac{2B_1+B_2}{M_0}\right]u_z=0\ , \tag{25}$$

$$\frac{(C_{11}+C_{12}+2C_{44})}{2}\frac{\partial u_x}{\partial x}-\frac{\sqrt{2}}{3}\left[\frac{B_1-B_2}{M_0}\right]m_y+M_0h_z+H_0m_z=0\ , \tag{26}$$

$$\frac{(C_{11}-C_{12}+4C_{44})}{6}\frac{\partial u_y}{\partial x}-\frac{\sqrt{2}(C_{11}-C_{12}-2C_{44})}{6}\frac{\partial u_z}{\partial x}-\frac{\sqrt{2}}{3}\left[\frac{B_1-B_2}{M_0}\right]m_x-\frac{1}{2\gamma' V}\frac{\partial \mu_z}{\partial t}=0\ , \tag{27}$$

and

$$\frac{(C_{11}-C_{12}+C_{44})}{3}\frac{\partial u_z}{\partial x}-\frac{\sqrt{2}(C_{11}-C_{12}-2C_{44})}{6}\frac{\partial u_y}{\partial x}+\frac{1}{3}\left[\frac{2B_1+B_2}{M_0}\right]m_x=0\ . \tag{28}$$

A small driving surface stress proportional to the electric field just inside the metal and to the electron mean free path could be added to the right-hand side of Eqs. (26)–(28). These terms' magnitude could be adjusted to account for the fact that, after collision with the metal's surface, the inertia of the electrons does not allow the current to be described by Eq. (20). Thus there is a surface layer of about an electron's mean-free-path thickness in which the lattice experiences a relatively large electric field which is not canceled by the electronic collision force. Also, depending on whether the electrons are specularly or diffusely reflected from the surface, there is a surface stress due to the electron collisions with the surface. Southgate[22] has shown that this is the physical mechanism which gives rise to the direct electromagnetic generation of sound in ordinary metals. These terms are far too small, however, to account for the experimentally observed sound generation in ferromagnetic metals.

The fields inside the material are conveniently written in terms of the z component of magnetic field for each wave, using the relations

$$f_\alpha=\sum_{j=1}^{14}Z(f_\alpha,k_j)h_z(k_j)\ , \tag{29}$$

where

$$f_\alpha\in\{h_x,h_y,h_z,m_x,m_y,m_z,u_x,u_y,u_z,e_y,e_z\}\ .$$

The $Z(f_\alpha,k_j)$ in Eq. (29) can be regarded as generalized impedances and are readily obtained from Eqs. (1), (2), (4), (10), (11), (13)–(15), and (21) once the k_j are known. The 18 boundary conditions result in 18 linear, inhomogeneous equations for the two reflected, two transmitted, and 14 waves within the magnetic material in terms of the amplitude of the incident electromagnetic wave. The determination of the k_j and subsequent solution of the boundary-value equations for the wave amplitudes are easily carried out by computer.

The solutions to the boundary-value problem indicate that there are four principal types of transmission. For the configuration with the incident microwave magnetic field perpendicular to the static field there is a peak in the magnetic-field-dependent transmission for one electromagnetic wave if the static field satisfies the ferromagnetic antiresonance condition.[23] For a limited range of frequencies there is also an enhancement in the transmission at ferromagnetic resonance due to sound transmission through the slab.[24,25] This transmission is attributable to the magnetoelastic coupling and is strongest at ferromagnetic resonance since that is where the transverse magnetization is largest. For the configuration with the microwave magnetic field parallel to the static field, the direct transmission of microwaves dominates the transmission through thin slabs, i.e., for slabs only a few skin depths thick. For thicker slabs sound waves are responsible for the transmission. There is no regime with the model considered for which the transmission is determined by spin waves.

V. DISCUSSION OF CALCULATION

The calculated transmission through a ferromagnetic slab in the configuration of Fig. 1 is dominated by the ordinary electromagnetic wave and longitudinal sound wave within the slab. The ordinary electromagnetic wave is, of course, what one would have in the case of a simple metal. The sound wave is present largely because the third term of Eq. (26) allows the electromagnetic field to exert a substantial stress on the lattice. The electromagnetic wave is heavily damped and, for a sufficiently thick slab, the transmission is primarily due to the relatively unattenuated sound wave.

The role played by the sound wave is most easily seen in the approximation that the material obeys Ohm's law with a scalar conductivity σ, the electron collision force and Lorentz force on the lattice cancel exactly, the magnetoelastic constants B_1 and B_2 are zero, and the slab is so thick that the waves reflected from the back surface are of negligible amplitude when they reach the front surface. In this case the relevant equations of motion decouple and one requires only two pairs of propagation constants.

At the front surface the incident electromagnetic wave gives rise to a reflected electromagnetic wave and to a sound wave and an electromagnetic wave transmitted into the metal. From Eqs. (23) and (26) and the continuity of h_z at the slab's surface one readily finds that the amplitude of the sound wave generated at the front surface is

$$u_x\approx\frac{2iM_0h_0}{(\omega\sqrt{\rho C})}[1-(1+i\omega^2/\omega_0^2)^{-1}]\ , \tag{30}$$

where

$$\omega_0=\sqrt{2}v_s/\delta=4\pi\sigma(v_s/c)^2\ . \tag{31}$$

In Eq. (31) δ is the skin depth and v_s is the speed of sound. For iron at room temperature and for sound propagating in the [110] direction, ω_0 corresponds to 75 MHz. At this frequency the sound wavelength and skin depth are comparable. Smaller terms in the denominator of Eq. (30) have been omitted under the assumption that $C \gg 4\pi M_0^2$ where $C=(C_{11}+C_{12}+2C_{44})/2$. Equation (30) is slightly different than Eq. (6) of Alexandrakis and Dewar[4] since that equation was based on Privorotskii's[16] work and his calculated stress improperly included a term proportional to the applied field. The applied field is included here in the fourth term of Eq. (13) and it effectively renormalizes the speed of sound.

The source of the sound calculated in Eq. (30) is essentially the third term of Eq. (26). The coupling between the electromagnetic wave and the sound wave is quite small and one could calculate to zeroth order the amplitude of the electromagnetic wave transmitted into the metal without considering the sound. Then the amplitude of the sound wave could be approximately obtained by treating the $M_0 h_z$ of Eq. (26) as a stress driving the sound wave, where the h_z is basically the electromagnetic wave's amplitude. For an incident electromagnetic wave of amplitude 1 Oe, the stress on iron is about 3.5×10^3 dyn/cm^2.

The average acoustic power generated per unit area of the metal is

$$P_s=\tfrac{1}{2}\sqrt{\rho C}\,\omega^2 |u_x|^2 . \tag{32}$$

The radiation efficiency η_f is the ratio of acoustic power generated to incident microwave power. Thus

$$\eta_f \approx \frac{16\pi M_0^2}{c\sqrt{\rho C}} \approx 10^{-9}, \quad \frac{v_s}{l} \gg \omega \gg \omega_0 \tag{33}$$

and

$$\eta_f \approx 16\pi M_0^2 \omega^4 / c\omega_0^2, \quad \omega \ll \omega_0 . \tag{34}$$

The numerical estimate in Eq. (33) applies to iron at a temperature of 110 K. (See Table I.) This is somewhat smaller than the efficiency of generation of gigahertz sound in metals via other mechanisms but is nonetheless substantial.[26] The upper limit on frequency in Eq. (33) is imposed by the condition that the electronic mean free path be much shorter than a sound wavelength. This is really too stringent (see below) and can be replaced by the requirement that the mean free path be less than the skin depth, i.e., $c^2/2\pi\sigma l^2 \gg \omega$.

The transmission at the back surface of a thick slab is easily calculated within the same approximation which led to Eq. (30). A longitudinal sound wave of amplitude u_{0_x} gives rise to a transmitted electromagnetic wave and reflected sound and electromagnetic waves. The amplitude of the transmitted electromagnetic wave is

TABLE I. Parameters used in the calculation of transmission through an iron single-crystal slab at 110 K.

$d=19$ μm	$C_{11}=2.4044\times10^{12}$ dyn/cm [c]
$\omega=5.8905\times10^{10}$ s^{-1}	$C_{12}=1.3687\times10^{12}$ dyn/cm [c]
$g=2.088$ [a]	$C_{44}=1.2113\times10^{12}$ dyn/cm [c]
$\sigma=4.1\times10^{17}$ s^{-1} [b]	$K_1=5.34\times10^5$ erg/cm^3 [i]
$\rho=7.9170$ g/cm^{-3} [c,d]	$K_2=0.0$ erg/cm^3
$4\pi M_0=22\,057$ G [e]	$B_1=-3.92\times10^7$ erg/cm^3 [j]
$\chi=1.06\times10^{-4}$ emu/Oe cm^3 [e]	$B_2=1.040\times10^8$ erg/cm^3 [j]
$\lambda=7.0\times10^7$ s^{-1} [f]	$A=2.19\times10^{-6}$ erg/cm [k]
$\alpha=1.88\times10^{-5}$ K^{-1} [d]	$n=5.1\times10^{22}$ cm^{-3} [l]
$C_p=2.39\times10^6$ erg/g [g]	$l=4.22\times10^{-6}$ cm
$\left(\frac{\partial\mu}{\partial T}\right)_{H,P}=-1.36\times10^{-2}$ emu/g [e]	$\Lambda=+3.16\times10^{-3}$ [m]
$\frac{1}{V}\left(\frac{\partial V}{\partial H}\right)_{P,T}=4.29\times10^{-10}$ Oe^{-1} [h]	$\frac{1}{nec}=+1.1\times10^{-25}$ s cm^2/esu [m,n]

[a] Z. Frait, Czech. J. Phys. B **27**, 185 (1977).
[b] Determined from Matthiessen's rule using the sample's measured residual resistivity ratio of 15.2 and the data of G. K. White and S. B. Woods, Philos. Trans. R. Soc. London, Ser. A **251**, 273 (1959).
[c] J. A. Rayne and B. S. Chandrasekhar, Phys. Rev. **122**, 1714 (1961).
[d] F. C. Nix and D. MacNair, Phys. Rev. **60**, 597 (1941).
[e] R. Pauthenet, J. Appl. Phys. **53**, 8187 (1982).
[f] S. M. Bhagat, L. L. Hirst, and J. R. Anderson, J. Appl. Phys. **37**, 194 (1966).
[g] K. K. Kelley, J. Chem. Phys. **11**, 16 (1943).
[h] E. Fawcett and G. K. White, J. Appl. Phys. **38**, 1320 (1967).
[i] P. Escudier, Ph.D. thesis, University of Grenoble, 1973.
[j] E. du Tremolet de Lacheisserie and R. Memdia Monterroso, J. Magn. Magn. Mater. **31-34**, 837 (1983).
[k] M. W. Stringfellow, J. Phys. C **1**, 950 (1968).
[l] This corresponds to 0.6 conduction electron per atom.
[m] R. W. Klaffky and R. V. Coleman, Phys. Rev. B **10**, 2915 (1974).
[n] Hall constant used only in Eq. (21).

$$h_t \approx 8\pi M_0 u_{0_x} \left[\frac{i\omega}{c}\right]\left[\frac{1+i\beta\omega^2/\omega_0^2}{1+i\omega^2/\omega_0^2}\right] . \quad (35)$$

The radiation efficiency at the back surface, η_b, is the ratio of the transmitted microwave power to the incident acoustic power. Thus

$$\eta_b \approx \frac{16\pi M_0^2\beta^2}{c\sqrt{\rho C}} \approx 6\times 10^{-10}, \quad c^2/2\pi\sigma l^2 \gg \omega \gg \omega_0 . \quad (36)$$

For the case $\omega \ll \omega_0$, replace β with 1 in Eq. (36). Note that this radiation efficiency at high frequency is independent of the magnetization of the material, since $M_0^2\beta^2$ is independent of M_0. The numerical estimate applies to iron at 110 K.

The efficiencies at the front and back surfaces are clearly not equal, especially if $\omega \ll \omega_0$. Most papers concerned with the calculation of the electromagnetic generation of sound deal with η_f only, whereas most papers concerned with the experimental aspects of sound generation contain the assumption $\eta_f = \eta_b$. This assumption is based upon notions of reversibility of energy flow. In the simplified calculation above there are three electromagnetic waves and one sound wave at the front surface and two electromagnetic and two sound waves at the back surface. It is impossible to map one set of waves into the other merely by reversing the direction of energy flow.

From Eqs. (30) and (35) the transmission amplitude through a thick slab for which multiple reflections are unimportant is

$$h_t \approx \frac{16\pi M_0^2\beta h_0}{c\sqrt{\rho C}} \approx 8\times 10^{-10} h_0 ,$$

$$c^2/2\pi\sigma l^2 \gg \omega \gg \omega_0 . \quad (37)$$

The amplitude in Eq. (37) should be further reduced according to the amount of attenuation the sound wave undergoes in traversing the slab. The full calculation yields transmission results which are within 1 part in 10^4 of that of Eq. (37) provided the attenuation of the wave as it traverses the sample is properly accounted for. Thus the transmission in the parallel-parallel configuration in thick slabs is due primarily to the longitudinal sound wave and depends on the spatially inhomogeneous Zeeman energy and the volume magnetostriction. The imbalance between the Lorentz force on the lattice and the electronic collision force plays a very small role in this transmission.

VI. COMPARISON WITH EXPERIMENT

In this section we compare the calculations with the results of experiments performed by Alexandrakis and co-workers[4–6] as well as some experiments of Blackstead and co-workers[7,8] which are relevant to these calculations.

The full transmission calculation outlined in Sec. IV is shown as the solid line in Fig. 2 as a function of applied, static magnetic field. Parameters used in the calculation are given in Table I. Shown also is the experimental transmission data obtained with a single crystal of iron 19 μm thick at a temperature of 110 K. The sample had the [110] direction normal to its plane and the static and microwave magnetic fields were along the [1$\bar{1}$1] direction. The average experimental transmission between 5.0 and 10.0 kOe has been normalized to 10 as has the calculated transmission at 7.5 kOe. Both the experiment and calculation are in good agreement and show very little magnetic field dependence for fields above 2 kOe. Since the [1$\bar{1}$1] direction is a hard axis in iron, the applied magnetic field must be at least as large as the anisotropy field before the sample becomes a single domain with the magnetization parallel to the applied field. For this reason the calculation has not been extended below 490 Oe. The plots of transmission versus magnetic field are similar to Fig. 2 at all temperatures studied (5–300 K).[5]

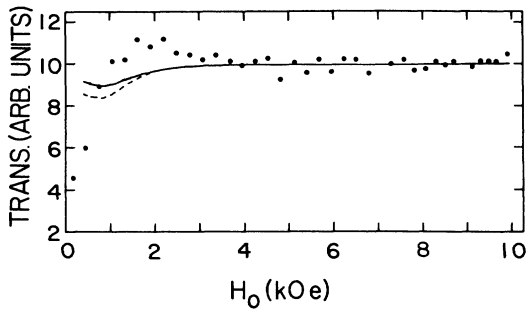

FIG. 2. Transmission amplitude vs applied magnetic field. Experimental data are for a [110]-oriented iron single-crystal 19 μm thick. The data were taken at 110 K. The average transmission amplitude between 5.0 and 10.0 kOe has been normalized to 10. The solid line was calculated using the parameters in Table I. The dashed line was calculated with the parameters of Table I except the volume magnetostriction was 2.0×10^{-8} Oe^{-1} and electronic attenuation of 40 times the free-electron attenuation was added to the longitudinal sound wave. Both calculated transmission curves have been normalized to 10 at 7.5 kOe.

The slight dip in the calculated transmission at ≈ 1 kOe is due to ferromagnetic resonance. The magnetoelastic coupling allows the sound wave to drive the transverse magnetization, Eqs. (10) and (13). Thus the longitudinal sound wave has some spin-wave character and ferromagnetic resonance affects the damping of the sound wave. For applied fields between 1 and 3 kOe the experimental data lie somewhat above the calculation. This suggests that the applied field is slightly misaligned with the [1$\bar{1}$1] axis and some transmission due to transverse sound waves is present.[27]

O'Donnell *et al.*[7] did pulse echo experiments with nickel at 4.2 K which demonstrated the generation of longitudinal phonons in the parallel-parallel configuration. Their samples were polycrystalline and one requires applied fields of several kilo-oersteds to overcome the magnetocrystalline anisotropy and magnetize the sample parallel to the applied field. Also, their samples were probably in the anomalous skin effect regime which

is beyond the scope of the calculations made here. However, the physical mechanisms which lead to the interconversion of phonons and microwaves are still present at these low temperatures. The saturated signal level in their Fig. 1 for fields ≥ 4 kOe is most probably due to the Zeeman force and volume magnetostriction. At smaller fields the sample is not magnetized to saturation and there is a component of the magnetization perpendicular to the applied field. This leads to sound generation through the magnetoelastic coupling. The variation of this perpendicular magnetization with field is most likely the reason for the complicated field dependence of the phonon signal for 0 kOe < applied field < 4 kOe.

The work of Blackstead and co-workers on gadolinium[8] was on single crystals. Their qualitative results, that the longitudinal phonon power was linearly proportional to incident microwave power and strongest when the microwave and static magnetic fields were parallel, are in agreement with the calculations presented here.

The calculated transmission through a magnetically saturated sample at applied fields far from ferromagnetic resonance versus conductivity can also be compared to experiment.[5] However, two modifications must be made to the calculation in order to make direct comparisons. First, the samples are not perfect slabs but are, in fact, slightly convex as a result of the polishing process they undergo. This nonuniform thickness makes it impossible for standing sound waves to be set up over the whole area of the sample exposed to microwaves. In contrast the calculation shows strongly enhanced transmission if an integral number of half wavelengths of sound match the slab's thickness. For the calculations shown in Fig. 3 the transmissions through slabs over a range of thickness were averaged together in order to approximate the transmission through a sample of nonuniform thickness. This is a fairly accurate approximation provided the nonuniformity is smooth, as it is with these samples. However, care must be taken to ensure that there is no resonance at any thickness used in the calculation since these resonances can be quite sharp and large and do not appear in the experimental data.

Second, the condition that $kl \ll 1$, where k is the propagation constant for sound, is not well satisfied in the experiment. ($kl = 1$ at $\sigma \approx 10^{18}$ s^{-1}.) This results in the calculation yielding the wrong attenuation for sound. The propagation constant has a small imaginary part which is primarily due to joule losses associated with the sound wave's small electric field and current. This should be augmented by an amount which describes the losses incurred by the electronic distribution as it tries to follow the modulation of the Fermi surface caused by the passage of the sound wave. Pippard[28] showed that, within the free-electron model, the ultrasonic attenuation for longitudinal waves can be expressed as

$$\mathrm{Im}k = \frac{(ne)^2}{2\sigma\sqrt{\rho C}} \left[\frac{1}{3} \frac{k^2 l^2 \tan^{-1}(kl)}{kl - \tan^{-1}(kl)} - 1 \right] . \quad (38)$$

Inclusion of deformation potentials alters and complicates this expression.[29] However, Eq. (38) does give an adequate description of the ultrasonic losses if the right-hand side is multiplied by a scale factor which is experimentally determined. For example, a scaled version of Eq. (38) adequately describes the ultrasonic attenuation in aluminum for a wide range of kl, with the largest discrepancy[30] being 20% at $kl = 1$. The essential point for our purposes is that the attenuation is readily shown from Eq. (38) to be proportional to conductivity[28] for $kl \ll 1$ and to be independent of conductivity for $kl \gg 1$. (It is possible that other mechanisms contribute to the ultrasonic losses, for example, dislocation damping, but the electronic dissipation alone was adequate to describe the data.)

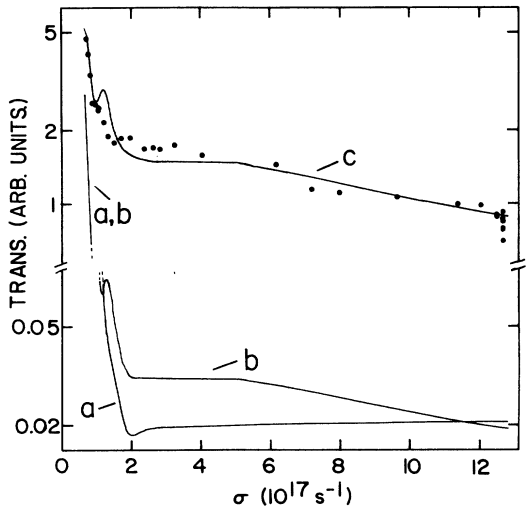

FIG. 3. Transmission amplitude (log scale) vs conductivity. The experimental data are for a 19 μm thick, [110]-oriented, iron single crystal. Each data point is the average transmission amplitude for applied fields between 5.0 and 10.0 kOe. The calculated curves are the equally weighted averages of transmission calculations for 100 slab thickness uniformly spaced between 19.10 and 19.25 μm. The calculations were done for an applied field of 5.0 kOe and, except as noted, used parameters from the references in Table I. Curve a is from Eq. (37). Curve b is the full calculation with electronic attenuation of 40 times the free-electron attenuation added to the longitudinal sound wave. Curve c is the same as b except the volume magnetostriction was 2.0×10^{-8} Oe^{-1}. The experimental data have been normalized to the calculation by requiring curve c to pass through the three lowest conductivity data points.

The calculation was modified so that the C_{ij}'s included a small imaginary part which, from the first term of Eq. (13), yielded a k which had its imaginary part proportional to the right-hand side of Eq. (38). This results in quite small relative changes in k and in $Z(f_\alpha,k)$, both of which enter the boundary equations. Since the difference between the local and nonlocal conductivities is small for the sound wave, the solution to the boundary equations of Sec. IV is little changed and is approximately the same as one would obtain using a fully nonlocal calculation such as that of Rodriguez and co-workers.[31] The electromagnetic wave's impedance is, however, pro-

foundly affected by whether the conductivity is local or nonlocal. Thus the calculation is reliable provided $kl \ll 1$ for the electromagnetic wave, i.e., $c^2/2\pi\sigma l^2 \gg \omega$. This condition is reasonably well met in the experiment.

The uniformly weighted average of 100 transmission calculations at 5 kOe versus conductivity for slab thicknesses equally spaced between 19.10 and 19.25 μm is shown in Fig. 3. Curve *a* is a calculation based on Eq. (37) and the temperature-independent parameters of Table I. (The other temperature-dependent parameters were interpolated from the references of Table I.) For $\sigma < 1\times10^{17}$ s^{-1} the transmission is dominated by the electromagnetic wave; for $\sigma > 3\times10^{17}$ s^{-1} the transmission is dominated by the longitudinal sound wave. Between these two conductivity values the two waves produce an interference pattern which is largely washed out by averaging over different thicknesses of slab. The slight temperature dependence of the magnetization, elastic constants, and volume magnetostriction determine the implied conductivity dependence of the transmission for $\sigma \geq 3\times10^{17}$ s^{-1}. This accounts for the weak increase in transmission at the larger conductivities.

Curve *b* of Fig. 3 is the full calculation with multiple reflections and it includes electronic damping of the sound wave corresponding to 40 times the free-electron damping. The sound transmission of curve *b* is greater than curve *a* for moderate conductivities because the sound damping is so light that multiple reflections are important. Curve *c* is the same as curve *b* except the volume magnetostriction is 2.0×10^{-8} Oe^{-1}.

Experimental data on a [110]-oriented single crystal are also shown in Fig. 3. Each data point represents the average transmission amplitude between 5.0 and 10.0 kOe. All but the three lowest conductivity data points, which are clearly due to electromagnetic transmission, are from previously published work.[5] The break between the steep electromagnetically dominated transmission and the flatter sound-dominated transmission occurs at $\sigma \approx 1\times10^{17}$ s^{-1} whereas the break in curves *a* and *b* occurs at $\sigma \approx 2\times10^{17}$ s^{-1}. Also, absolute calibration of the transmission apparatus, although imprecise, indicates that the experimental amplitudes are at least an order of magnitude greater than the calculations for curves *a* and *b*.

The calculated sound transmission is primarily determined by iron's magnetization, elastic constants, and volume magnetostriction. It is not possible that this excessive transmission is due to a resonance with the slab's thickness being an integral number of sound half-wavelengths. The elastic constants change sufficiently over the temperature range used to sweep out conductivity that such a resonance would appear as a peak in Fig. 3. Such a peak is not evident in the data.

It is plausible that the volume magnetostriction is sensitive to the amount of damage introduced into the iron during the sample-preparation procedure. After the samples were cut from an oriented single-crystal iron rod they were mechanically polished with diamond grit. This yielded flat, parallel sides on the samples. The finest grade of diamond grit used was 3-μm grit and this produced damage which decreased with distance from the surface with a scale length of ≈ 3 μm. Much of this damage was removed by chemically polishing the samples to their final thickness. Unfortunately the chemical polishing procedure resulted in samples with a slightly convex shape. In order to preserve the flat, parallel-sided sample geometry as much as possible, the amount of material removed with the chemical polish was judiciously limited and some damaged material remained after polishing.

In order to get the calculated break in the transmission curve to agree with the data, as well as to get reasonable agreement between the relative amplitudes of the electromagnetic and sound transmission, the volume magnetostriction used in the calculation must be increased to ≈ 50 times the bulk value, as shown by curve *c*. The experimental data were normalized to curve *c* by requiring that curve to pass through the three lowest conductivity data points.

The large volume magnetostriction used to fit the experimental data has little effect on the shape of the sound transmission curve, as can be seen by comparing curves *b* and *c* for $\sigma > 3\times10^{17}$ s^{-1}. This part of curves *b* and *c* is primarily determined by the value of the sound attenuation. Changing this attenuation to 30 or 50 times the free-electron value results in curves which clearly disagree with the data. The sound attenuation of curve *c* corresponds to 0.05 dB/μm at 298 K and to 0.2 dB/μm at 110 K. These values are somewhat lower than those of Homer *et al.*[6] since he did not consider the effect of multiple reflections in that work.

VII. CONCLUSIONS

The experimental microwave frequency transmission through a ferromagnetic metal plate is well described by a calculation incorporating equations of motion for the lattice and magnetization. For the case in which the incident microwave magnetic field is parallel to the applied, static field and the plate is thick, the transmission is dominated by sound traversing the plate. This longitudinal sound is generated through the stress which results from the inhomogeneous Zeeman energy at the ferromagnet's surface. The reconversion of sound to microwaves at the plate's back surface is crucially dependent on the volume magnetostriction being nonzero. Neither the magnetoelastic coupling constants B_1 and B_2, the Lorentz force and the electronic collision force on the lattice, nor the ferromagnetic Hall effect play any significant role in this transmission. Further, the interchange of angular momentum between the lattice and the magnetic carriers necessitated by the nonzero volume magnetostriction has no discernible effect on the transmission.

The comparison of the experimental data to the calculation indicates that the electronic attenuation of 9.4-GHz sound in iron is about 0.05 dB/μm at room temperature and is proportional to conductivity. The data are in agreement with the assumption that the attenuation is electronic in nature and is approximately 40 times

the free-electron value. Also, the transmission is sensitive to the condition of the sample's surface and implies that the volume magnetostriction can be increased by damage introduced by mechanical polishing of the iron crystal.

ACKNOWLEDGMENTS

The author is indebted to J. Nearing and G. C. Alexandrakis for valuable advice given during the development of the work presented here.

[1]K. Myrtle, B. Heinrich, and J. F. Cochran, J. Appl. Phys. **52**, 2250 (1981).
[2]B. Heinrich and J. F. Cochran, J. Appl. Phys. **52**, 1811 (1981).
[3]G. C. Alexandrakis, R. A. B. Devine, and J. H. Abeles, J. Appl. Phys. **53**, 2095 (1982).
[4]G. C. Alexandrakis and G. Dewar, J. Appl. Phys. **55**, 2467 (1984).
[5]G. Dewar and G. C. Alexandrakis, J. Appl. Phys. **57**, 3733 (1985).
[6]R. Homer, G. C. Alexandrakis, and G. Dewar, J. Appl. Phys. **61**, 4133 (1987).
[7]M. O'Donnell, S. C. Hart, J. G. Sylvester, and H. A. Blackstead, Solid State Commun. **18**, 1141 (1976).
[8]M. O'Donnell, J. T. Wang, and H. A. Blackstead, Phys. Rev. Lett. **36**, 606 (1976).
[9]H. F. Tiersten, J. Math. Phys. (N.Y.) **5**, 1298 (1964).
[10]C. Vittoria, G. C. Bailey, R. C. Barker, and A. Yelon, Phys. Rev. B **7**, 2112 (1973).
[11]T. Kobayashi, R. C. Barker, J. L. Bleustein, and A. Yelon, Phys. Rev. B **7**, 3273 (1973).
[12]C. Vittoria, J. N. Craig, and G. C. Bailey, Phys. Rev. B **10**, 3945 (1974).
[13]M. B. Salamon, Phys. Rev. **155**, 224 (1967).
[14]L. Kraus and Z. Frait, Czech. J. Phys. B **23**, 188 (1973).
[15]J. F. Cochran, B. Heinrich, and G. Dewar, Can. J. Phys. **55**, 787 (1977).
[16]A. Privorotskii, Phys. Lett. **69A**, 53 (1978).
[17]E. R. Dobbs, in *Physical Acoustics,* edited by W. P. Mason and R. N. Thurston (Academic, New York, 1973), p. 127.
[18]C. Kittel, *Introduction to Solid State Physics,* 4th ed. (Wiley, New York, 1971), p. 145.
[19]L. Berger, Phys. Rev. B **2**, 4559 (1970).
[20]T. Kjeldaas and T. Holstein, Phys. Rev. Lett. **2**, 340 (1959).
[21]M. H. Cohen, M. J. Harrison, and W. A. Harrison, Phys. Rev. **117**, 937 (1960).
[22]P. D. Southgate, J. Appl. Phys. **40**, 22 (1969).
[23]B. Heinrich and V. F. Meshcheryakov, Pis'ma Zh. Eksp. Teor. Fiz. **9**, 618 (1969) [JETP Lett. **9**, 378 (1969)].
[24]J. W. Allen and G. C. Alexandrakis, Solid State Commun. **27**, 251 (1978).
[25]B. Heinrich and J. F. Cochran, J. Appl. Phys. **50**, 2440 (1979).
[26]Y. Goldstein and A. Zemel, Phys. Rev. Lett. **28**, 147 (1972).
[27]G. Dewar and G. C. Alexandrakis, J. Appl. Phys. **53**, 8116 (1982).
[28]A. B. Pippard, Philos. Mag. **46**, 1104 (1955).
[29]A. B. Pippard, Proc. R. Soc. London, Ser. A **257**, 165 (1960).
[30]B. Berre, Phys. Rev. B **30**, 4130 (1984).
[31]G. Feyder, E. Kartheuser, L. R. Ram Mohan, and S. Rodriguez, Phys. Rev. B **25**, 7141 (1982).